



FLOW FEATURE VISUALIZATION USING LOGICAL OPERATORS ON MULTIVARIATE FIELDS

Ralf P. Botchen *, Andreas Lauser *, Daniel Weiskopf **, Thomas Ertl *

*Institute for Visualization and Interactive Systems

Universität Stuttgart, Universitätsstraße 38, Stuttgart, Germany

{botchen|lauser|ertl}@vis.uni-stuttgart.de

**Visualization Research Center Universität Stuttgart

VISUS, Nobelstr. 15, Stuttgart, Germany

weiskopf@visus.uni-stuttgart.de

KEYWORDS:

Main subject(s): *Flow Visualization*

Fluid: *Incompressible Fluids*

Visualization method(s): *Feature Visualization*

Other keywords: *First-Order Logic*

ABSTRACT: *Due to the large size of high-dimensional datasets that result from contemporary computational flow simulations, the classification and visualization of features is an essential, though challenging task for proper scientific analysis. We present a visualization system based on first-order fuzzy logic, that allows to convert natural language statements involving multiple scalar properties into well defined features which can be used for that allows to define and combine multiple feature criteria as logic visualization using geometric primitives in conjunction with the underlying flow field. A feature criterion can be defined as an atomic point predicate, which can be understood as a function, that maps all data points of a dataset to a Boolean value. Boolean algebra can then be used to combine these atomic predicates to define more complex ones. The combination of several feature criteria to one characteristic subset can be used to build one single geometric isosurface representation of several features, and thus, significantly reduce the amount of graphical primitives needed to display all features separately, minimizing clutter and occlusion. Further, the created subset can be utilized for particle seeding, with the aim to show the behavior of the flow in the surrounding area. We evaluate the positive and negative aspects of two different types of logical operators for the example of different simulation datasets and several feature criteria.*

1 Introduction

Vector fields and their associated scalar fields that emerge from flow simulation often contain millions of data values. Even for rather small datasets with only a couple thousand data values, a direct examination of the data with the intention to find certain features is almost impossible for the analyst. This fact leads to the need to reduce the large data flood and present only desired details of the data to the viewer. The research areas on flow analysis, feature extraction and flow feature visualization has put forth significant work over the last two decades. The demand of investigating multivariate flow fields has actually expanded from scientific research to engineering disciplines and led to a multitude of feature extraction techniques that work on scalar and vector fields, causing the necessity of visualization systems that can display the features and the flow field simultaneously.

In general, a feature is a prominent attribute or aspect that characterizes something of interest. As proposed by Peikert [18], a flow feature can be classified by its locality or dimensionality and thus, characterizes a set of points in a multivariate field, defined by a given feature criterion. For example, feature extraction methods can be based on criteria like vortex core lines [24], vortex core regions [1], ridge lines, valley lines, or separation lines [12], but also other properties like pressure, temperature and uncertain or erroneous data values [17] can be of interest for the analyst. Once features are defined and extracted, one of the challenges for adequate visualization techniques is the capability of illustrating a combination of multiple features at a time to give a structural overview, without making the application too complex. One possible approach for this purpose is the use of a higher level of abstraction to represent the data as done by flow topology methods [14], although these methods are mostly limited to work on singularities of the underlying field. Another approach is to partition the flow field based on user-defined properties [21] and to display the flow structures only in regions that fulfill these conditions.

In this paper, we present a flow feature visualization system using first-order fuzzy logic (FOFL) for a combined analysis, as shown in the work flow diagram of Figure 1. The system allows the user to define and combine multiple feature criteria as logic point predicates and display the resulting characteristic set as isosurface with geometric primitives. For this purpose, the work flow of the system is subdivided into three layers that can be interacted with by the user; (1) feature definition and extraction, (2) logical combination of feature sets and (3) visualization of the structures created by the feature sets in combination with the surrounding flow behavior. As shown in [21], for first-order logic (FOL), an atomic point predicate P can be understood as a function that maps all data points of a dataset domain D to a Boolean value $P : D \in \mathbb{R}^3 \rightarrow \{\text{true}, \text{false}\}$, $x \mapsto P(x)$. Boolean algebra can be used to combine these atomic predicates to define more complex ones. However, for the combination of features, this might not be sufficient enough, since FOL is restricted to a binary decision, but a feature criteria is mostly given by a fuzzy extent. This gives rise to the use of FOFL [21], holding two advantages. First, the resulting set is a fuzzy set too, stating not only whether the combination exists, but also how well it applies. Second, we are interested in building geometry to graphically illustrate the feature set to the user. The fuzzy set can be used as input to a geometry construction algorithm like Marching-Cubes [3], whereby the user has the possibility to choose the iso-value for extraction. For this purpose, the conjunction of several feature criteria to one resulting set is convenient, since it reduces the amount of graphical primitives needed to display all features separately, and thus minimizes clutter and occlusion. Starting to reduce this characteristic feature set, we support seeding and tracing of particles to include the behavior of the underlying flow field as context information into the visualization. This technique can be used as valuable tool by analysts to support the understanding of interesting regions in datasets with less effort. Further, this approach is also appropriate to verify the results of different feature extraction approaches by means of similarity. We evaluate the aspects of two different types of logical operators, i.e. min/max logic and multiplicative logic for feature visualization.

2 Related Work

The work in this paper is based on feature extraction and flow visualization for the purpose of detection and analysis of combined feature characteristics in multivariate flow fields. While feature detection and tracking is an interesting field that has been investigated for a long time, less research has been conducted on combined feature visualization and analysis. We give an overview on both areas in the following.

In flow visualization, a multitude of research has focused on the detection of vortices, which belong

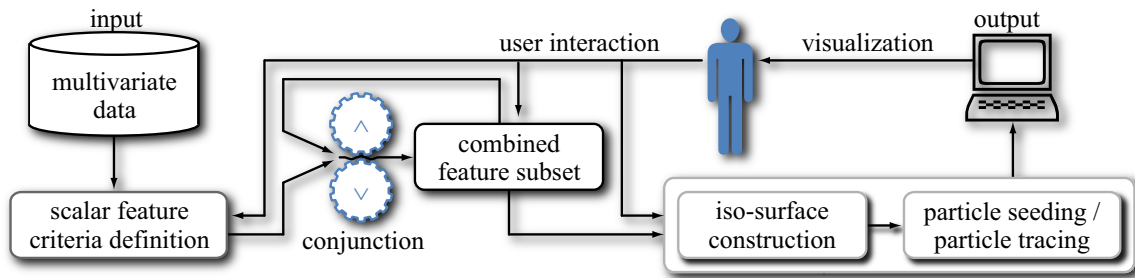


Fig. 1 The work flow of the proposed system consists of three layers: (1) feature definition, (2) logical feature combination and (3) feature visualization.

to the most important criteria for analyzing 3D fields from computational fluid dynamics (CFD). The essential problem for all vortex detection methods is the absence of an explicit and unique definition of a vortex. Thus, all approaches employ flow attributes that describe a rotation or a swirling motion around a center of a region, leading to a line-based or a region-based description of the vortex.

Among the line-based approaches, Banks and Singer [1] introduced a method that uses high absolute vorticity and low pressure to detect and trace the vortex core. They trace in the direction of the vorticity vector and search for a pressure minimum in the normal plane that is used as new vortex position. Sujudi and Haines [24] work on tetrahedral cells, computing the Jacobian of the interpolant and using the real eigenvector to find the velocity zero points to compose the vortex lines. Peikert and Roth [18] proposed a second order method using the parallel vector concept on a pair of vector fields, for defining global line-type features. They detect zero curvature of those two fields on a per cell basis and connect those locations to form a vortex core line.

For region-based approaches, there exist typical methods like the λ_2 criterion by Jeong and Hussain [10]. This method decomposes the Jacobian into the symmetric part S and the antisymmetric tensor Ω . In regions where the resulting symmetric tensor of $S^2 + \Omega^2$ has two negative eigenvalues, they assume a vortex and reconstruct the vortex region. In [13], Levy *et al.* introduced a helicity based method by supposing the location of a vortex core in regions where the angle between velocity and vorticity vectors approaches ± 1 . In [2], Banks and Singer presented a method for approximating a vortex skeleton around a prior extracted vortex core line.

After extraction, the segmentation of flow features plays an important role for feature tracking in unsteady flow fields. Region growing methods [11] have been widely used for this purpose in 3D volumes. Pattern matching with the Gabor filter [6] and Clifford convolution has been employed to segment the flow field. Further, Chen *et al.* [4] proposed the feature tree data structure which allows the tracking to work between refinement levels, time steps and processors.

More research on other features includes boundary layers and wakes, as presented by Haines and Kenwright [9]. They use the norm of the second principal invariant of the stress deviator as a measure of shear. An enhanced shear layer representation was presented by Meyer [16] lately. Here, the kinematic decomposition of the velocity field is considered in the neighborhood of a point, to draw conclusions about the shear stress. We use the approach by Haines in our work to define predicates for shear layers. An extensive overview and comparison of feature extraction methods is given in [18]. Once a feature is extracted, an efficient combination and visualization of multiple features is essential for a proper analysis. Doleisch *et al.* [5] developed a framework for flexible and interactive specification of high-dimensional features. They use the brush metaphor as selection method, which allows the user to choose a subset of features by painting with a brush-like tool on the domain of all extracted features. Sauber *et al.* [23] used a multi-field graph to visualize correlations in various scalar data.

The correlations are defined by the similarity of the gradients calculated from the different fields. Salzbrunn and Scheuermann [21] map features to functions that return a Boolean value for every point in the dataset, giving the information whether a point belongs to a certain feature. They create streamline predicates with functions that tell the user about the connection between streamlines and features selected by the user. In [20], they carried on their work to pathline predicates, allowing the definition of structures for unsteady flow. An complete overview of state-of-the-art feature extraction and visualization approaches can be found in the survey of Post *et al.* [19]. Our work extends the ideas of using predicates and logical operators for flow features. Unlike in [21], where a set of streamlines is computed and then, each streamline is accepted or neglected by checking whether it applies to the defined predicate, we first create a logical combined subset of features and build up a geometrical representation, to use it as a basis for particle seeding. On the one hand, this saves computation time for the particle traces, since we only compute valid streamlines and on the other hand, we highlight the region of the feature set by illustrating it as geometry in conjunction with the streamlines of underlying flow, to enhance the process of analysis.

3 Definition of Feature Criteria

As a first step for feature based visualization, proper feature extraction methods are essential. Thus, an important task is to find an appropriate definition that leads to a good detection and thereupon to an adequate representation of the desired feature. There exist a multitude of features for flow fields and scalar fields as listed in the previous section, whereby the extraction is mostly done as a semi-automatic preprocessing step and after extraction often only one feature class is visualized.

For an interactive analysis, the question of what is or is not considered to be a feature eventually refers to the user and depends on what part of the data the user is interested in. Further, features can be either global or local; the former are influenced by all values of the field, whereby the latter represent a local quantity. However, both are a characterization of a set of points. Therefore, the definition of a feature is usually closely coupled to the dataset that is to be analyzed.

In our system, features are extracted semi-automatically from the given dataset and result in a normalized scalar field, i.e. the fuzzy domain of the feature. In principle, any possible criteria can be defined, as long as it can be mapped to a scalar field. Though, so far the system supports a limited subgroup of important feature extraction methods, as given below. On the resulting scalar fields the user is then in a position to interactively define and combine several desired feature criteria for illustration during analysis.

3.1 Examples for Feature Criteria

3.1.1 Vortices

Vortices are among the most relevant features in a flow for many applications. We identify the vortex regions using the λ_2 method by Jeong and Hussain [10]. For a given velocity field

$$v_i(x_i + dx_i) = v_i(x_i) + \frac{\partial v_i}{\partial x_j} dx_j, \quad (1)$$

where v_i is the velocity vector, x_i the position, dx_i the displacement vector to an infinitesimal neighboring point in the fluid and $\frac{\partial v_i}{\partial x_j} = v_{i,j}$ is the velocity gradient. The λ_2 scalar is computed by first decomposing the Jacobian matrix of the velocity field – i.e. the velocity gradient tensor $v_{i,j}$ – into the symmetric part S and the antisymmetric part Ω

$$v_{i,j} = \frac{1}{2}(v_{i,j} + v_{j,i}) + \frac{1}{2}(v_{i,j} - v_{j,i}) = S_{ij} + \Omega_{ij}. \quad (2)$$

From a physical point of view, S is the strain-rate tensor and Ω the vorticity tensor. In the next step, the eigenvalues of the matrix $S^2 + \Omega^2$ have to be determined. Since this matrix is real and symmetric, it results in three eigenvalues — the roots of the characteristic polynomial — denoted by $\lambda_1 \geq \lambda_2 \geq \lambda_3$. A vortex is then defined as a connected region where two of the eigenvalues are negative, meaning that we use the normalized absolute value of λ_2 as scalar feature criterion.

3.1.2 Shear Layers

Boundary layers or shear layers are important, since they embody two kinds of features that can lead to meaningful conclusions. On the one hand, they tell that the fluid is under shear stress and on the other hand, they also indicate the generation of vorticity. This suggests a marker that is a function of both Ω and shear. As shown in [9], the stress tensor contains both the bulk and the shear stress and is independent on the coordinate system. To extract a single scalar that is coordinate system invariant and has the bulk terms removed it is necessary to diagonalize this tensor. The result is always three real eigenvalues $(\lambda_{s1}, \lambda_{s2}, \lambda_{s3})$, that produce a vector which signifies the principle axis of deformation. The norm of the second principal invariant of the stress deviator can be used as a measure of the shear. This is denoted as

$$\sqrt{\frac{(\lambda_{s1} - \lambda_{s2})^2 + (\lambda_{s1} - \lambda_{s3})^2 + (\lambda_{s2} - \lambda_{s3})^2}{6}}. \quad (3)$$

Using only the two strongest eigenvalues empirically gives better results. Therefore Eq. 3 reduces to $\lambda_s = \lambda_{s1} - \lambda_{s2}$. A scalar shear field s_H can then be constructed from a function of $|\Omega|$ and λ_s .

3.1.3 Scalar Attributes and Derived Quantities

Although scientists and engineers are primarily interested in the overall flow behavior, depending on the requirements of the application domain, other attributes can be of importance. Therefore, the system supports the analysis of various fields like pressure p or density ρ and derived quantities like velocity magnitude $\|v_i\|$ or vorticity magnitude $\|\omega_i\|$. Further, for an efficient understanding of a real-world measured data, it can be important to indicate how accurate and reliable the measuring system and thus the visualized data is, since there are a number of possibilities how the acquired data can be affected by uncertainty or error [8, 17]. In a related context, results from different simulation algorithms need to be compared in order to show variances in critical regions. We denote the scalar uncertainty criterion as η in the following.

4 Using First-Order Fuzzy Logic to Define Characteristic Sets

In the second stage, we use predicates to formulate functions on the characteristic feature sets with logical operators $\{\neg, \wedge, \vee\}$. The difficulty of using standard FOL is its binary nature, meaning that a predicate can either be true or false. Yet, most feature extraction methods do not classify the feature in a Boolean way, but rather give a fuzzy version of a characteristic feature set that tells about the extent of the feature. Therefore, fuzzy point predicates are employed to indicate whether a feature exists to a certain extend at a given location of the dataset, meaning that we can describe a continuous connected region as feature. Predicates of valence 1 express statements like high pressure exists and are used to operate and extract features from the data. Therefore, all implemented predicates operate on a normalized range and the continuous FOFL fulfills the following three conditions:

1. It is consistent with binary Boolean logic $P(x) = \{\text{true}, \text{false}\}$.
2. The De Morgan's rules hold for all possible values.
3. Operators must be continuous functions.

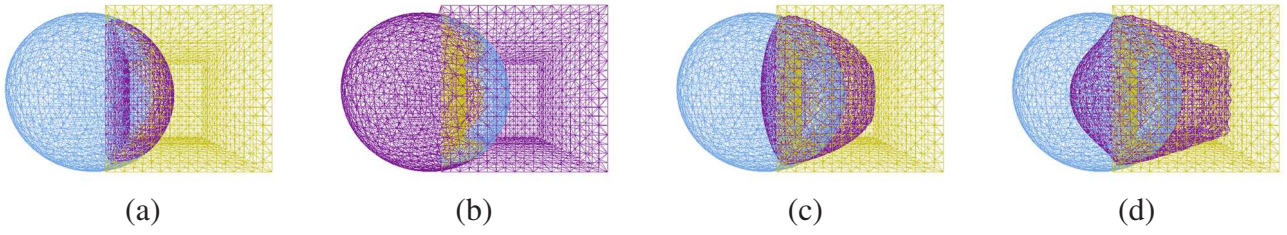


Fig. 2 Images (a,b) illustrate the results of the C^0 -continuous min/max-logic for an artificial iso-value dataset consisting of a sphere overlapped by a cube. The conjunction \wedge is shown in (a), and the disjunction \vee in (b). Images (c,d) show the results of the C^∞ -continuous multiplicative logic, with the conjunction \wedge^* in (c), and the disjunction \vee^* in (d) respectively.

For the a feature criterion ξ given on the domain D_ξ , a fuzzy predicate \mathcal{P}_ξ and a combined characteristic set CS are defined as follows:

$$\mathcal{P}_\xi : D_\xi \rightarrow [0, 1], \quad CS = \bigcup_{\mathcal{P}_\xi(D_\xi) > 0} D_\xi.$$

Here, ξ may represent λ_2 , s_H , $\|v\|$, $\|\omega\|$, p , ρ or η and the fuzzy value represents the extent of a feature at a given point. We show results for two different logic approaches – min/max logic and multiplicative logic operators – and evaluate the positive and negative aspects of those operators, when applied to flow visualization.

Min-Max Logic

The operators for min-max logic are defined as follows:

$$\begin{aligned} \mathcal{P}_{\xi_k} \wedge \mathcal{P}_{\xi_l} &= \min\{\mathcal{P}_{\xi_k}, \mathcal{P}_{\xi_l}\} \\ \mathcal{P}_{\xi_k} \vee \mathcal{P}_{\xi_l} &= \max\{\mathcal{P}_{\xi_k}, \mathcal{P}_{\xi_l}\} \\ \neg \mathcal{P}_\xi &= 1 - \mathcal{P}_\xi. \end{aligned}$$

Multiplicative Logic

The second type of operators we use in our system implements multiplicative logic, leading to the following definition of operators:

$$\begin{aligned} \mathcal{P}_{\xi_k} \wedge^* \mathcal{P}_{\xi_l} &= \sqrt{\mathcal{P}_{\xi_k} \cdot \mathcal{P}_{\xi_l}} \\ \mathcal{P}_{\xi_k} \vee^* \mathcal{P}_{\xi_l} &= \neg(\neg \mathcal{P}_{\xi_k} \wedge^* \neg \mathcal{P}_{\xi_l}) \\ \neg \mathcal{P}_\xi &= 1 - \mathcal{P}_\xi. \end{aligned}$$

From a geometrical point of view, the min-max logic is equivalent to set operations on isosurfaces and is in general C^0 -continuous. This is adequate for geometry construction algorithms, that we apply later on, since they are commonly C^0 -continuous too. However, from the combinational point of view, the results of min-max logic might not be satisfactory enough. One of its characteristics – i.e. the stronger or weaker feature dominates the result – can completely neglect the other one and thus, lead to a loss of information. Here, the use of multiplicative logic can be advantageous, because of its C^∞ -continuous nature. This means, that the resulting set of a combination covers a region, that is influenced by all participating features. The effect of the different behavior for the two logics are illustrated in Figure 2. The example shows the concatenation of two artificial feature sets representing a sphere (blue) and a cube (yellow). Both features increase from their barycenter, the isosurfaces was build with an iso-value of 0.5. The result of the respective operation is colored in purple.

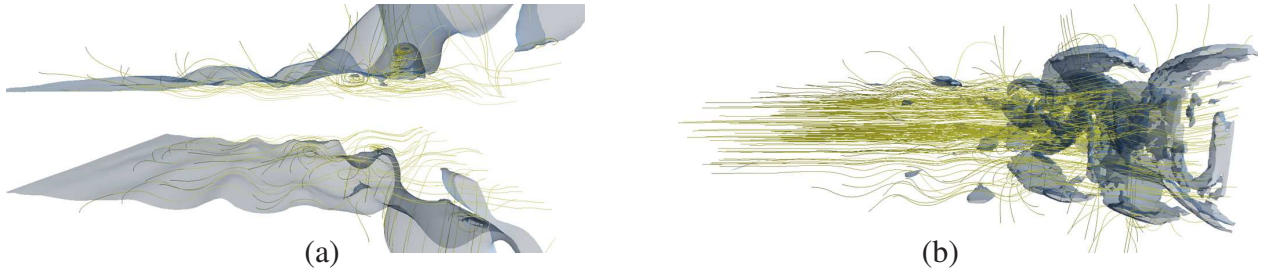


Fig. 3 The images illustrate the structural results for feature extraction on the ejection nozzle dataset for low velocity magnitude $CS = \mathcal{P}_{\|v\|} = 0.1$ (a) and high vorticity magnitude $CS = \mathcal{P}_{\|\omega\|} = 0.9$ (b).

5 Interactive Feature-based Visualization for Analysis

The third stage provides visualization by giving a structural overview of the extracted feature sets in combination with an illustration of the surrounding flow behavior as streamlines. Depending on the underlying dataset, different aspects of the data can be of interest to the user. In general, engineers have a basic idea about what kind of features are important for them and how to define and combine them to obtain a reasonable characteristic feature set. However, an accurate representation of the desired feature set is often achieved by repeatedly tuning the parameters — usually done by adjusting the iso-value c for the surface construction, the placement of the seed points, or the length of the traced lines — and, thus, for an interactive analysis there should be the possibility to customize the feature sets to the users needs. The system enables the interactive modification of parameters for feature extraction. Based on the characteristic feature set, we then build the structural overview with 2D geometric primitives and 1D tracelines.

The extracted features are given as fuzzy point set which can be simplified and described quantitatively in order to be visualized by geometry. Therefore, we use the hull of the feature set, given by the user defined threshold value c to build the isosurface by means of $\{\forall T \exists G : CS_T = c\}$. Here, c is the iso-value that gives information of how good the feature applies. Choosing a high value leads to geometry in regions where this feature dominates, a low value results in geometry in regions with low extent respectively. Since we work on tetrahedral grids this implies, that for all tetrahedra T we construct a geometric primitive G , if the isosurface runs through it. The construction of the geometry is computed with the Marching-Tetrahedra algorithm [25], an adapted version of the more common Marching-Cubes algorithm [3]. Once the surface grid is computed, it is used as source for particle tracing. As seeding strategy, we place a particle on the barycenter of every n -th grid polygon — whereby n can be specified by the user — to adequately cover the feature domain. Outgoing from their initial seeding position, the particles are traced forward and backward with the second order Runge-Kutta method. A bonus of this elementary approach is that it avoids the problems of occlusion and clutter that can occur, when seeding particles in the whole domain and thus, the user can directly explore the flow behavior in regions of interest by a sparse seeding on the chosen feature domain. On the other hand — as shown in Figure 3 (a,b) for low $\|v\|$ and high $\|\omega\|$ — the choice of a single non combined feature set can cause the particle tracing to miss important parts of the flow.

6 Results and Discussion

We have tested our system with three datasets coming form different engineering application scenarios. Figure 4 shows the spatial evolution of a liquid sheet, ejected at Reynolds number of 4,000 from a diverging ejection nozzle. The DNS volume-of-fluid simulation of the liquid was done with the focus to find the most instability enhancing parameters and to give detailed information on the possible

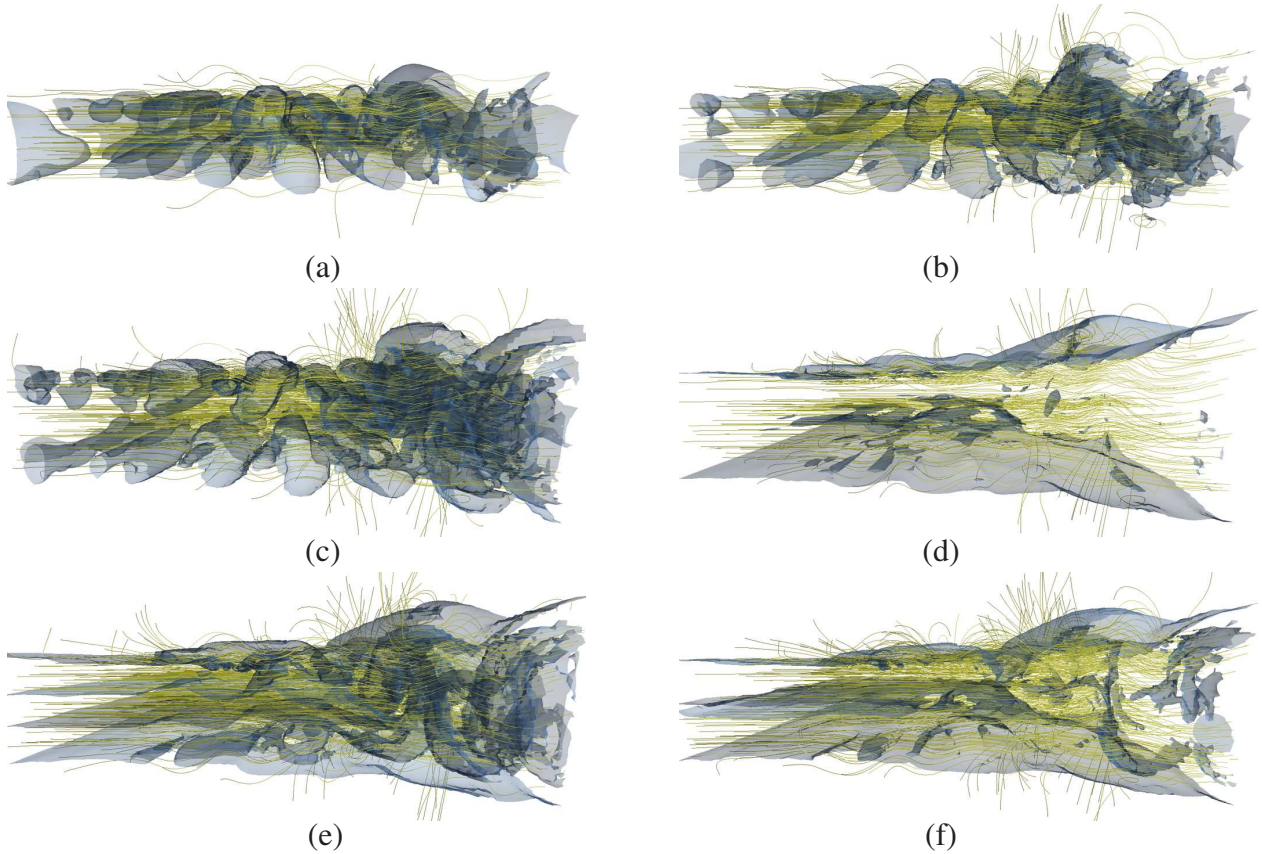


Fig. 4 Illustration of the ejector nozzle dataset with the corresponding extracted feature sets: (a) $CS = \mathcal{P}_p = 0.1$, (b) $CS = \mathcal{P}_{\lambda_2} \wedge^* \mathcal{P}_p = 0.1$, (c) $CS = \mathcal{P}_{\lambda_2} = 0.1$, (d) $CS = \mathcal{P}_{s_H} \wedge^* \mathcal{P}_{\|v\|} = 0.1$, (e) $CS = \mathcal{P}_{s_H} = 0.1$, (f) $CS = (\mathcal{P}_{\lambda_2} \wedge^* \mathcal{P}_p) \vee^* (\mathcal{P}_{s_H} \wedge^* \mathcal{P}_{\|v\|})$.

outcome concerning the spreading rate and the disintegration mechanism depending on the character of the nozzle. The dataset was computed by the Institute of Aerospace Thermodynamics, at the Universität Stuttgart. It was simulated on a Cartesian grid with $480 \times 384 \times 192$ resolution and 253 time steps. The dataset we used for testing shows time step 220, converted to 64,000 tetrahedral cells. As presented in [22], the nature of flow through converging or diverging channels is strongly influenced by the angle and the length of the nozzle, basically leading to an acceleration or a deceleration of the flow. Though the diverging nozzle type represents only a very small technical modification compared to a parallel nozzle, a very high level of kinetic energy flux of $\varepsilon = 1.55$ can be achieved, leading to a typical sinusoidal wave instability. The fuzzy predicates used to create the characteristic sets for images (a), (c) and (e) are based on p , λ_2 and s_H , respectively. In image (b) we used the combination $CS = \mathcal{P}_p \wedge^* \mathcal{P}_{\lambda_2}$, leading to a thinned out but very similar result compared to images (a) and (c). This feeds the assumption that low pressure and the existence of vortical regions is directly coupled. For image (d) the characteristic set is defined as $CS = \mathcal{P}_{s_H} \wedge^* \mathcal{P}_{\|v\|}$, showing that low speed and shear mainly appears in the boundary region of ejected fluid and surrounding air. In Figure 4 (f), the multiplicative disjunction of the results presented in image (b) and (d) lead to a geometric representation that adequately covers the domain for particle seeding, while providing information of the presence of all four used features.

The water channel dataset presented in Figure 5 was obtained in a real world experiment designed for studying laminar-turbulent boundary layer transitions in a water channel. The measurements, conducted by the Institute for Aerodynamics and Gasdynamics at the University of Stuttgart, consist of a $81 \times 45 \times 9$ hexahedra-based dataset acquired with the PIV method. Since our visualization

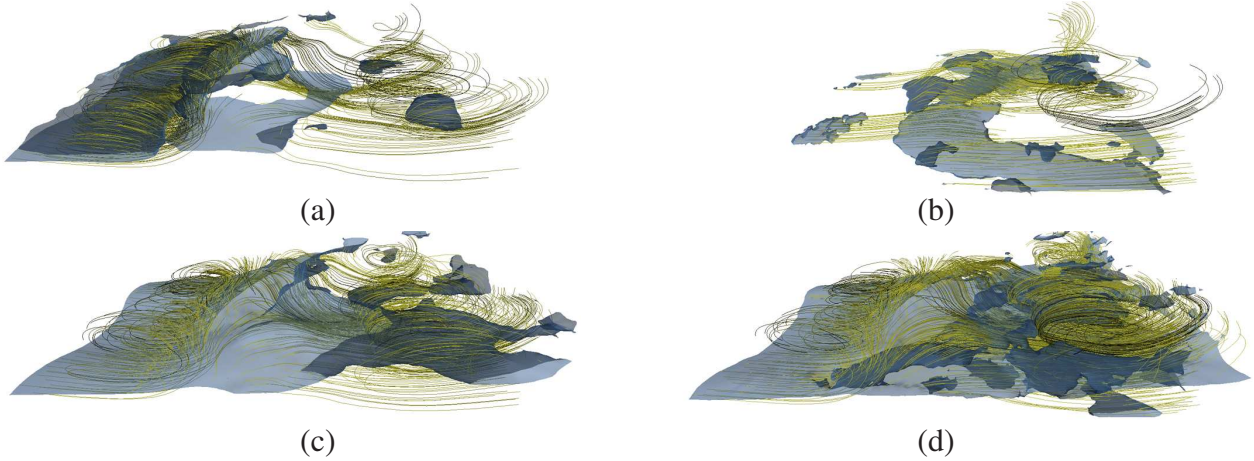


Fig. 5 Laminar water channel with rendered characteristic sets: (a) $CS = \mathcal{P}_{\|v\|} \vee \mathcal{P}_{s_H} = 0.05$, (b) $CS = \mathcal{P}_{\|v\|} \wedge \mathcal{P}_{s_H} 0.05$, (c) $CS = \mathcal{P}_{\|v\|} \vee^* \mathcal{P}_{s_H} = 0.05$, (d) $CS = \mathcal{P}_{\|v\|} \wedge^* \mathcal{P}_{s_H} 0.05$.

system was designed for tetrahedral grids, it was necessary to resample the original data set with 16,000 tetrahedral cells. Further information on the acquired original data can be found in [15]. Image (a) in Figure 5 shows the isosurface rendering with particle traces for the min-max disjunction of velocity magnitude and shear and in (b) the corresponding min-max conjunction. As described before, this type of logical combination leads to a result that totally neglects the counterpart. Nevertheless, it reveals that the velocity magnitude at the inlet region on the left side is higher than on the right side (a), whereas a higher shear value dominates the bottom region on the right (b). In contrast to that, we show the domain filling multiplicative disjunction in (c) and the multiplicative conjunction in (d). The continuous results of multiplicative logical operations lead to a structural feature representation that adequately covers the region to unveil the flow properties of interest, whereby the conjunction certainly covers more of the domain.

The wall-mounted finite cylinder data sets illustrated in Figures 6 and 7 was computed on an unstructured grid with 12.3 million grid points, for both LES and DES. We resampled both datasets with 64,000 tetrahedral cells. The simulation for both original data sets was performed on the same grid with a Reynolds-number of 200,000. The final data is averaged, using 3083 single time steps. Computation timings for the cylinder data sets are given for a cluster computer with 42 IBM pSeries 690 PCs with 1.3 GHz. For the 12.3 million grid points, it took the cluster 3.1 minutes for LES and 5.0 minutes for DES per simulated time step. More details on the original data sets and its acquisition can be found in [7]. The visualization of the DES and LES simulations is an example of comparative visualization, i.e., the difference between different simulation results serves as uncertainty measure η . To give an insight of the structures formed by single features, Figure 6 (a-d) shows the extractions for λ_2 and s_H as side and top view. A combination of high λ_2 and high uncertainty is illustrated in Figure 6 (e-f). Note, that therefore λ_2 needs to be inverted, as by definition, a smaller value covers more of the vortical region. Figure 7 (a-f) displays logical combinations of λ_2 , s_H , η , $\|v\|$ and $\|\omega\|$. The multiplicative disjunction of negated shear and negated uncertainty results in an isosurface that excludes the uncertain regions but includes the high shear near the bottom, as can be seen in the top view of Figure 7 (b). With more sophisticated combinations as in images (e,f) it becomes clear that regions where all features are combined have a large extend are in the direct neighborhood of the cylinder.

As can be seen from the resulting images, the use of one single feature as seeding source can lead to a very cluttered visualization as in images (c) and (e) of Figure 4, as the feature has a high occurrence in the data, or the lack of the feature results in a few sparsely distributed seeding points as in images

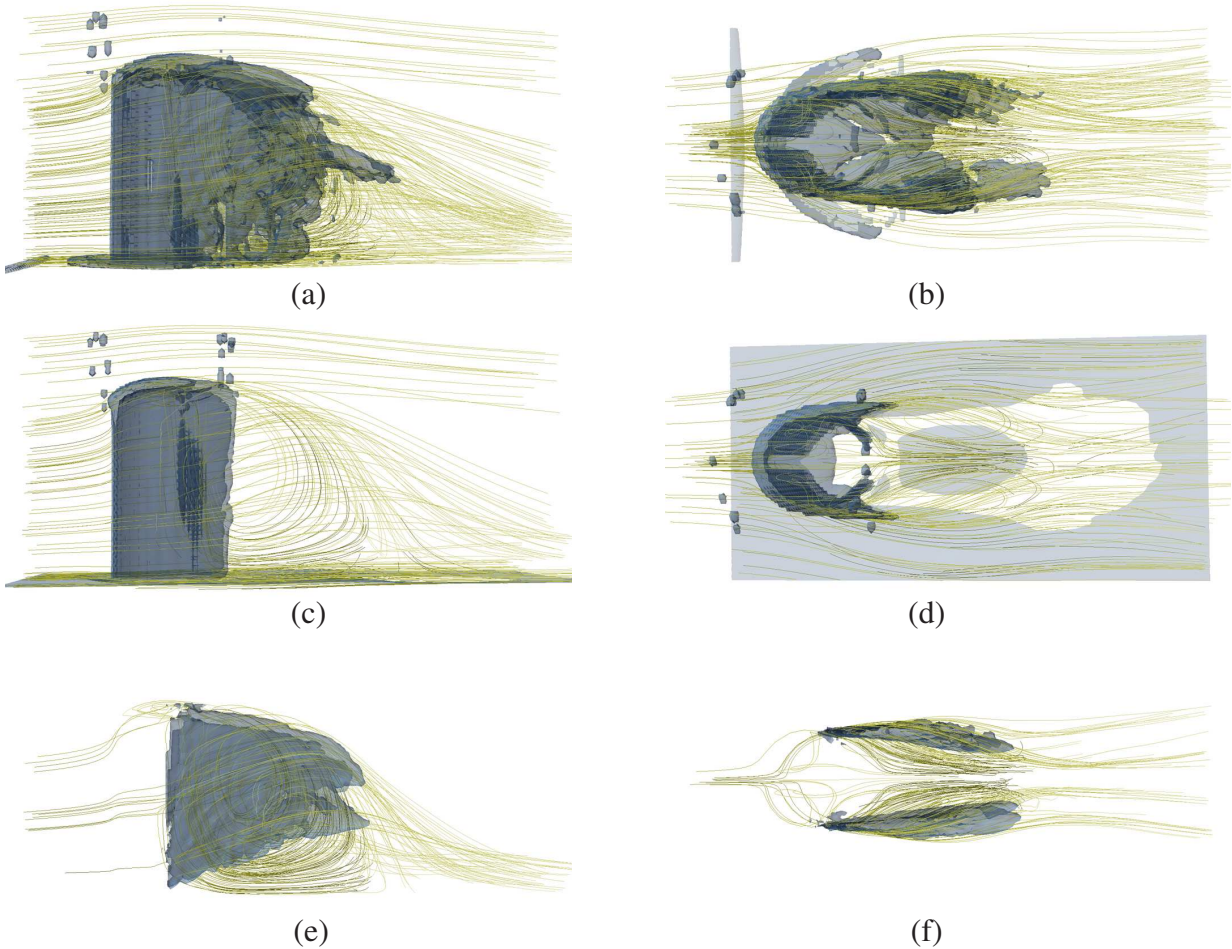


Fig. 6 The wall mounted cylinder rendered with single feature sets from side and top view: (a,b) $CS = \mathcal{P}_{\lambda_2} = 0.15$, (c,d) $CS = \mathcal{P}_{SH} = 0.1$, (e,f) $CS = \neg \mathcal{P}_{\lambda_2} \wedge \mathcal{P}_{\eta} = 0.9$.

of Figure 6 (c-f). Thus, a sophisticated user defined combination of multiple desired features can give a good structural overview of all regions where these features appear, as well as an adequate amount of seeding geometry, that can be adjusted by the user.

7 Conclusions and Future Work

We have presented a system for the interactive analysis of flow fields, based on a flexible combination of user defined feature criteria. Starting from the extracted feature sets an investigation of the surrounding flow behavior has been employed by placing particles on the characteristic feature hull and tracing streamlines on the field. We see this as a useful tool to cope with multivariate fields by representing them on a higher level of abstraction and to give the user the possibility to interactively steer the system during analysis. In future work, we intend to test our system with several other relevant attributes which includes an extension to handle vector based features. We are also looking for a possibility to create predicates that express the correlation of similar behavior in different fields.

Acknowledgements

The authors thank Wolfgang Sander for making the ejection nozzle dataset available, Octavian Friedrich for providing the different simulation data of the wall mounted cylinder and Matthias Lang for the laminar water channel measurements.

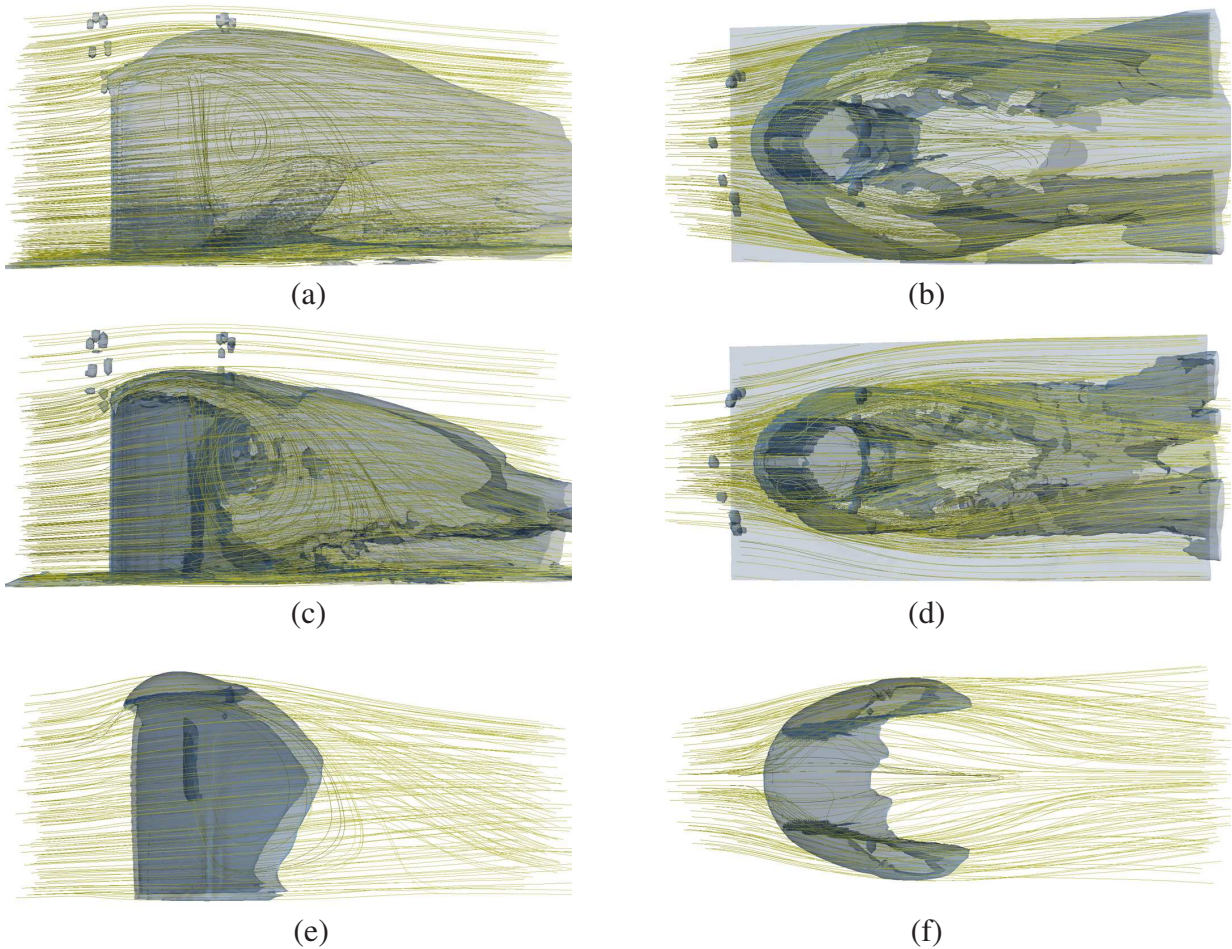


Fig. 7 The wall mounted cylinder illustrated with combined feature sets: (a,b) $CS = \neg \mathcal{P}_{s_H} \wedge^* \neg \mathcal{P}_\eta = 0.95$, (c,d) $CS = \neg \mathcal{P}_{s_H} \wedge^* \neg \mathcal{P}_\eta \wedge^* \neg \mathcal{P}_{\lambda_2} = 0.95$, (e,f) $CS = (\neg \mathcal{P}_{s_H} \wedge^* \mathcal{P}_{\|v\|}) \vee^* (\neg \mathcal{P}_{\lambda_2} \wedge^* \mathcal{P}_\eta \wedge^* \neg \mathcal{P}_{\|\omega\|}) = 0.9$.

References

- [1] D. C. Banks and B. A. Singer. Vortex tubes in turbulent flows: Identification representation, reconstruction. In *Proceedings of IEEE Visualization*, pages 132–139, 1994.
- [2] D. C. Banks and B. A. Singer. A predictor-corrector technique for visualizing unsteady flow. *IEEE Transactions on Visualization and Computer Graphics*, 2(1):151–163, 1995.
- [3] B. P. Carneiro, C. T. Silva, and A. E. Kaufman. Tetra-cubes: an algorithm to generate 3D isosurfaces based upon tetrahedra. In *Proceedings of the IX SIBGRAPI International Conference*, pages 205–210, 1996.
- [4] J. Chen, D. Silver, and L. Jiang. The feature tree: Visualizing feature tracking in distributed AMR datasets. In *Proceedings of IEEE Symposium on Parallel and Large-Data Visualization and Graphics*, pages 103–110, 2003.
- [5] H. Doleisch, M. Gasser, and H. Hauser. Interactive feature specification for focus+context visualization of complex simulation data. In *Proceedings of VISSYM '03*, pages 239–248, 2003.
- [6] J. Ebling and G. Scheuermann. Segmentation of flow fields using pattern matching. In *Proceedings of EuroVis*, pages 147–154, 2006.
- [7] O. Frederich, E. Wassen, and F. Thiele. Flow simulation around a finite cylinder on massively parallel computer architecture. In *Proceedings of the International Conference on Parallel Computational Fluid Dynamics*, Washington D.C., USA, 2005.

- [8] H. Griethe and H. Schumann. The visualization of uncertain data: Methods and problems. In *Proceedings of SimVis*, pages 143–156, 2006.
- [9] R. Haimes and D. Kenwright. On the velocity gradient tensor and fluid feature extraction. Technical Report 99-3288, AIAA, Norfolk, Virginia, 1999.
- [10] J. Jeong and F. Hussain. On the identification of a vortex. *Journal of Fluid Mechanics*, (285):69–94, 1995.
- [11] G. Ji, H.-W. Shen, and R. Wenger. Volume tracking using higher dimensional isocontouring. In *Proceedings of IEEE Visualization*, pages 209–216, 2003.
- [12] D. N. Kenwright. Automatic detection of open and closed separation and attachment lines. In *Proceedings of IEEE Visualization*, pages 151–158, 1998.
- [13] Y. Levy, D. Degani, and A. Seginer. Graphical visualization of vortical flows by means of helicity. *AIAA Journal*, 28:1347–1352, 1990.
- [14] K. Mahrous, J. Bennett, G. Scheuermann, B. Hamann, and K. Joy. Topological segmentation in three dimensional vector fields. *IEEE Transactions on Visualization and Computer Graphics*, 2(10):198–205, 2004.
- [15] O. Marxen, M. Lang, U. Rist, and S. Wagner. A combined experimental/numerical study of unsteady phenomena in a laminar separation bubble. *Flow, Turbulence and Combustion*, 71(1-4):133–146, 2003.
- [16] D. Meyer. *Discrete numerische Simulation nichtlinearer Transitionsmechanismen in der Strömungsgrenzschicht einer ebenen Platte*. Phd thesis, Luft- und Raumfahrttechnik, Universität Stuttgart, 2003.
- [17] A. T. Pang, C. M. Wittenbrink, and S. K. Lodha. Approaches to uncertainty visualization. *The Visual Computer*, 13(8):370–390, 1997.
- [18] R. Peikert and M. Roth. The parallel vectors operator - A vector field visualization primitive. In *Proceedings of IEEE Visualization*, pages 263–270, 1999.
- [19] F. H. Post, B. Vrolijk, H. Hauser, R. S. Laramée, and H. Doleisch. The state of the art in flow visualization: Feature extraction and tracking. 22(4):775–792, 2003.
- [20] T. Salzbrunn, C. Garth, G. Scheuermann, and J. Meyer. Pathline predicates and unsteady flow structures. *The Visual Computer (available as Online First article on springerlink.com)*, 2008.
- [21] T. Salzbrunn and G. Scheuermann. Streamline predicates. *IEEE Transactions on Visualization and Computer Graphics*, 12(6):1601–1612, 2006.
- [22] W. Sander and B. Weigand. Direct numerical simulation and analysis of instability enhancing parameters in liquid sheets at moderate reynolds numbers. *Physics of Fluids*, (accepted for publication).
- [23] N. Sauber, H. Theisel, and H.-P. Seidel. Multifield-graph: An approach to visualizing correlations in multifield scalar data. In *Proceedings of IEEE Visualization*, pages 917–924, 2006.
- [24] D. Sujudi and R. Haimes. Identification of swirling flow in 3d vector fields. Technical Report 95-1715, Department of Aeronautics and Astronautics, MIT, Cambridge, 1995.
- [25] G. M. Treece, R. W. Prager, and A. H. Gee. Regularised marching tetrahedra: improved iso-surface extraction. *Computers & Graphics*, 23(4):583–598, 1999.

Copyright Statement

The authors confirm that they, and/or their company or institution, hold copyright on all of the original material included in their paper. They also confirm they have obtained permission, from the copyright holder of any third party material included in their paper, to publish it as part of their paper. The authors grant full permission for the publication and distribution of their paper as part of the ISFV13/FLUVISU12 proceedings or as individual off-prints from the proceedings.